length like D_f, but rugosity or particles of different sizes.

In summary, we feel that the apparent flow-induced shear thickening observed by us and by others is, in fact, an elongational-flow-induced "coil–stretch" transition of the adsorbed macromolecules. Rugosity of the pore walls or irregularities in pore structure are necessary to produce the local elongational flow. We do not, however, want to insist that we have proven this. Besio et al.[15] have recently published the first study of elongational flow effects on polymer adsorption. Our opinion is that this kind of work is essential for clarifying the hydrodynamic behavior of adsorbed polymer layers in the presence of rugosity.

Acknowledgment. Matthew Tirrell thanks the National Science Foundation (PYI Program) and the John Simon Guggenheim Memorial Foundation for support of this work.

Registry No. PS, 9003-53-6; Pusher 700, 39341-25-8; Nuclepore, 12673-61-9.

References and Notes

(1) Rowland, F. W.; Eirich, F. R. *J. Polym. Sci., Polym. Chem. Ed.* **1966**, *4*, 2401.
(2) Chauveteau, G. Society of Petroleum Engineers, San Antonio Meeting, TX, 1981; Paper No. 10060.
(3) Gramain, P.; Myard, P. *Macromolecules* **1981**, *14*, 180.
(4) Chauveteau, G.; Tirrell, M.; Omari, A. *J. Colloid Interface Sci.* **1984**, *100*, 41.
(5) Cohen, Y.; Metzner, A. B. *Macromolecules* **1982**, *15*, 1425.
(6) Idol, M. K.; Anderson, J. L. *J. Membr. Sci.* **1986**, *28*, 269.
(7) Cohen, Y. *Macromolecules* **1988**, *21*, 494.
(8) Lee, J.-J.; Fuller, G. G. *Macromolecules* **1984**, *17*, 375.
(9) Fuller, G. G.; Lee, J.-J. *J. Colloid Interface Sci.* **1985**, *107*, 308.
(10) Chauveteau, G. *J. Rheol. (N.Y.)* **1982**, *26*, 111.
(11) Bohrer, M. P.; Fetters, L. J.; Grizzuti, N.; Pearson, D. S.; Tirrell, M. *Macromolecules* **1987**, *20*, 1827.
(12) Chauveteau, G. In *Water Soluble Polymers*; Glass, E. J. Ed.; Advances in Chemistry 213; American Chemical Society: Washington, DC, 1986; Chapter 14, p 227.
(13) Bagassi, M. Thèse, Université de Bretagne Occidentale, 1986.
(14) James, D. F.; Saringer, J. H. *J. Fluid Mech.* **1980**, *97*, 655; *J. Non-Newtonian J. Fluid Mech.* **1982**, *11*, 317.
(15) Besio, G. J.; Prud'homme, R. K.; Benzinger, J. B. *Macromolecules* **1988**, *21*, 1070.

Self-Consistent Field Model of Polymer Adsorption: Matched Asymptotic Expansion Describing Tails

Harry J. Ploehn and William B. Russel*

Department of Chemical Engineering, Princeton University, Princeton, New Jersey 08544.
Received December 23, 1987; Revised Manuscript Received May 31, 1988

ABSTRACT: General self-consistent field equations, derived previously, are solved within a perturbation scheme for the configuration probability of polymer chains. Building upon an earlier ground-state solution which describes adsorption in an "inner" region but precludes the prediction of tails, an "outer" region solution is developed herein as the lowest order term in a perturbation expansion of the configuration probability in powers of reciprocal chain length. This solution is asymptotically matched with the inner (ground state) solution, yielding a uniformly valid approximation. From this solution, we derive an analytical expression for the polymer volume fraction profile, including contributions due to segments contained in loops, tails, and nonadsorbed chains. Predictions for the adsorbed amount of polymer, ellipsometric layer thickness, and hydrodynamic layer thickness agree qualitatively with experimental data. We describe the variation of chain configuration statistics (e.g., the distribution of segments in trains, loops, and tails) with experimental parameters. These results are analyzed by using simple thermodynamic arguments.

Introduction

A considerable number of interesting and important materials and processes contain interfaces modified by a polymeric component. An extensive list of applications of this type, give by Eirich,[1] includes the stabilization and flocculation of colloidal suspensions. Such systems are dominated by interfacial effects; their stability and properties depend strongly upon the details of particle interactions, in this case mediated by adsorbed layers of polymer molecules. Naturally, an understanding of the interactions of adsorbed polymer layers requires a complete description of the configurations of the constituent molecules. This description is the object of most theories of polymer adsorption.

The earliest polymer adsorption theories consider isolated adsorbed molecules but have little practical relevance since even for weak adsorption energies, a large number of molecules may adsorb per unit area, resulting in significant intermolecule interaction. Nonetheless, valuable insights did emerge. For example, Hesselink[2] employed the random-walk formalism developed by Chandrasekhar[3] to calculate the number of possible configurations of isolated molecules attached to the surface by one or both end groups ("tails" and "loops", respectively). Idealizing a polymer molecule as a "chain" of "segments" exhibiting random-walk statistics, Hesselink found that a tail of n segments has $(2\pi n)^{-1/2}2^n$ possible configurations, while a loop of n segments may assume any of $(2\pi n)^{-1/2}2^n n^{-1}$ configurations. As Takahashi and Kawaguchi conclude in their review,[4] consideration of only configurational entropy implies that the existence of tails is favored over that of loops, especially for large n. This result contrasts sharply with many early and even some contemporary adsorption theories which (implicitly or explicitly) assume that polymer chains adsorb only in loops and "trains" (runs of adsorbed segments).

The most comprehensive and successful theory describing the random adsorption of homopolymers is the lattice model of Scheutjens and Fleer (SF). The SF theory, which has been described extensively,[5] treats a wide range of experimental conditions with no a priori assumptions about the configurations of adsorbed polymer chains. The predicted characteristics of the adsorbed layers agree qualitatively with much experimental data, but the model is limited in several respects. In particular, the SF model involves the discretization of space, necessitating the selection of a lattice geometry (i.e., simple cubic, hexagonal close packed, etc.) thay may not accurately reflect the

0024-9297/89/2222-0266$01.50/0

reality of continuous space. Furthermore, the model equations are cast in a finite difference form that facilitates numerical solution but obscures some of the underlying physics.

We attempt to overcome these problems through the formulation of a general self-consistent field theory derived from first principles.[6] The object of the calculation is the probability density $G(\mathbf{r},sl)$ that chains of s segments of length l end within $d\mathbf{r}$ of spatial position $\mathbf{r}$. Chain configuration statistics embodied in $G(\mathbf{r},sl)$ are described by a stochastic process model[10] based on a set of mathematical consistency conditions. Straightforward manipulation[3,6] of the consistency conditions produces a partial differential field equation for $G(\mathbf{r},sl)$. The field equation is, in fact, a form of the Schrödinger equation which includes a potential energy term that perturbs the random walk of the polymer chain from its ideal state. The potential field accounts for the energy of segment–segment, segment–solvent, and segment–surface interactions which determine the probability of chain configurations. Minimization of the total free energy of the system via the statistical mechanical analyses of Helfand[7] or Hong and Noolandi[9] identifies the form of the potential (its functional dependence on the local segment and solvent volume fractions) that is truly "self-consistent", that is, yields the equilibrium distribution of chain configurations. The same result may be obtained by using the "osmotic equation-of-state" described by Dickman and Hall.[8] These methods ensure that all segment interactions, both in the adsorbed layer and in bulk polymer solution, are treated consistently by using a single equation of state.

In our earlier work,[6] we find a solution of the general self-consistent field (SCF) equation for nonionic homopolymer adsorbing on a single, planar surface. First, we expand $G(\mathbf{r},sl)$ in the eigenfunctions of the Schrödinger equation. Keeping only the lowest order ground-state eigenfunction and linearizing the self-consistent potential field (except at the surface) lead to analytical solutions for the configuration probability G and the volume fraction of polymer segments as functions of spatial position. Within the ground-state approximation, though, the distribution of individual segments is independent of their rank within the chain: no end effects are predicted, and thus, tail configurations are precluded.

In this work we develop a solution of the polymer adsorption problem which recognizes the dual nature of an adsorbed layer. Close to the surface, chain configurations are grossly distorted from ideality by the attraction of the surface and interactions with neighboring chains. Far from the surface in bulk solution, the local configurations are those of random walks in a homogeneous potential field. The two regions are matched by rescaling the SCF equations with the appropriate characteristic lengths in each region and solving the resultant equations within a perturbation scheme. The matched solution is a uniformly valid approximation over the entire adsorbed layer. From this solution, we derive analytical volume fraction profiles for segments in loops, tails, and nonadsorbed chains; other results, including the adsorbed amount, the mean layer thickness, and the hydrodynamic thickness, are compared with experimental data. An analysis of configuration statistics indicates which features of adsorbed polymer layers are sensitive to variation of experimental parameters. Finally, we discuss the limitations of our approach.

Theory

Self-Consistent Field Equation. The goal of most polymer adsorption theories is the description of the structure of an adsorbed layer through statistical analysis of the configurations of the constituent polymer and solvent molecules. Rather than considering the location and orientation of each real polymer bond, the polymer is divided into a "chain" of statistical "segments" with the number of real bonds per segment chosen so that the chain exhibits random-walk statistics. The contour of a polymer chain embedded in an adsorbed polymer/solvent layer is analogous to the path of a diffusing particle under the influence of an external potential field. The rank of a segment (its contour position within a chain) replaces time. A polymer configuration is characterized by the set of spatial positions of each segment in the chain.

The problem of computing the statistics of chain configurations is most conveniently cast in the form of a stochastic process model.[10] A set of consistency conditions governs a hierarchy of probability densities giving the joint probabilities of finding sequences of segments in specified configurations. Although this description is complete, it is not tractable and simplifications are necessary. First, we assume that a segment's position depends only on the explicit position of the previous segment and the local potential field which accounts for all other interactions. Of course, this is a Markov process. Next, we assume that the potential acting on a segment has been "preaveraged" over the local probabalistic distribution of segments and solvent, i.e., the usual "mean-field" approximation.[11]

With these assumptions, it is tedious but not difficult[3,12] to derive a field equation for $G(\mathbf{r},sl)$. A heuristic exposition,[6] though, is informative and concise. Since $G(\mathbf{r},sl)$ is a Markov process, it can be expressed as the product of two probabilities: the probability $G(\mathbf{r}',l(s-1))$ that a walk of $s-1$ steps ends at a position $\mathbf{r}'$ such that $|\mathbf{r}-\mathbf{r}'| = l$ and the transition probability $e^{-\beta U(\mathbf{r})}$ that the final step leads from $\mathbf{r}'$ to $\mathbf{r}$ ($\beta = 1/kT$). $U(\mathbf{r})$ is the local mean potential field at $\mathbf{r}$ arising from the energy of a segment interactions. The product $e^{-\beta U(\mathbf{r})}G(\mathbf{r}',l(s-1))$ is integrated over the spherical locus of positions $\mathbf{r}'$ where the intersection can occur and normalized with $4\pi l^2$ to provide

$$G(\mathbf{r},s) = \frac{e^{-\beta U(\mathbf{r})}}{4\pi l^2}\int_S G(\mathbf{r}',l(s-1))\,d\mathbf{r}' \qquad (1)$$

a recursive integral equation for the configuration probability $G(\mathbf{r},s)$. In fact, (1) is the basic equation utilized in the SF theory[5] with the integral replaced by a summation over discrete lattice sites. Scaling spatial position and contour length on the segment length l, expanding $G(\mathbf{r}',s-1)$ in a Taylor series in $\mathbf{r}$ and s, and integrating over the sphere S produce the self-consistent field (SCF) equation

$$\frac{\partial G}{\partial s}(\mathbf{r},s) = \frac{1}{6}\nabla^2 G(\mathbf{r},s) + [1 - e^{\beta U(\mathbf{r})}]G(\mathbf{r},s) \qquad (2)$$

which is the fundamental equation to be studied herein.

The self-consistent field, $U(\mathbf{r})$, was originally formulated in its most general form by Helfand.[7] A more recent analysis by Hong and Noolandi[9] accounts for the translational entropy of finite length chains. The form of $U(\mathbf{r})$ that guarantees an equilibrium distribution of chain configurations in the adsorbed layer is

$$U(\mathbf{r}) = \frac{\partial}{\partial \rho_p}[f(\rho_p,\rho_s) - \rho_p\mu_p^{\,b} - \rho_s\mu_s^{\,b}] - \frac{kT}{n}\ln[\rho_p/\rho_p^{\,b}] = \Delta\mu_p \qquad (3)$$

where $f(\rho_p,\rho_s)$ is the local free energy density of a homogeneous solution with polymer segment and solvent number densities ρ_p and ρ_s; $\mu_p^{\,b}$ (on a per segment basis) and $\mu_s^{\,b}$ are the corresponding chemical potentials in bulk so-

lution where $\rho_p(\mathbf{r}) \rightarrow \rho_p^b$, a constant. In thermodynamic terms, U may be interpreted as the local excess chemical potential of segments ($\Delta\mu_p$). The free energy density in (3) accounts for the energy of all segment interactions and is provided by a polymer solution equation of state (discussed below).

Other heuristic arguments[6] or formal manipulation of the consistency conditions[12] yield the polymer volume fraction profile

$$\varphi(\mathbf{r}) = v_1\rho_p(\mathbf{r}) = \frac{c}{e^{-\beta U(\mathbf{r})}}\int_0^n G(\mathbf{r},s)G(\mathbf{r},n-s)\,ds \quad (4)$$

where v_1 is the volume of a segment, n is the total dimensionless chain length, and c is a constant that depends on the equilibrium state of the adsorbed layer. If the layer is in full equilibrium with bulk solution ($\varphi_b = v_1\rho_p^b$), then $c = \varphi_b/n$, since far from the surface, $\varphi \rightarrow \varphi_b$, $U \rightarrow 0$, and $G \rightarrow 1$. After $f(\varphi)$ is provided, the closed set of equations (2)–(4) may be solved by using standard mathematical techniques.

Self-Consistent Field. The choice of the polymer solution equation of state, which characterizes the energy of all segment interactions, is critically important. In previous work,[6] we employed the Flory equation of state[15] to calculate $U(\mathbf{r})$. Using the prescription of (3), the resultant (Flory) self-consistent field is identical with that found from the statistical mechanical analysis of Scheutjens and Fleer.[5] However, computer simulations[8,16] indicate that the lattice-based Flory equation severely underestimates the osmotic pressure of athermal solutions in a continuum. A more accurate equation is needed for our continuous-space calculations.

In this work, we model the polymer–solvent mixture as a pseudo-one-component fluid. For positions such that $\mathbf{r} \neq \mathbf{r}_0$, the compressibility factor has the van der Waals form

$$Z = \frac{(1 + \varphi + \varphi^2 - \varphi^3)}{(1 - \varphi)^3} - 8\alpha\varphi \quad (5)$$

where α is a polymer–solvent interaction parameter and $0 \leq \varphi(\mathbf{r}) \leq 1$. The first term in (5) is the Carnahan–Starling[17] compressibility factor for hard (athermal) spheres. For solutions other than athermal, entropic repulsion is augmented by a van der Waals-type attraction accounting for the energy of mixing segments with solvent. The solvent molecules are treated as a continuum and contribute no translational entropy to the fluid free energy.

The osmotic pressure Π is related to the compressibility factor Z through

$$\Pi/kT = Z\rho_p = Z\varphi/v_1 \quad (6)$$

and to the local free energy density $f(\rho_p)$ by

$$\Pi = \rho_p^2\frac{\partial(f/\rho_p)}{\partial\rho_p} = \varphi^2\frac{d(f/\varphi)}{d\varphi} \quad (7)$$

which can be integrated for f. Combining (3) and (5)–(7) produces

$$\beta U_c = -16\alpha\varphi + \frac{\varphi(8 - 9\varphi + 3\varphi^2)}{(1 - \varphi)^3} \quad (8)$$

as the SCF defined for $\mathbf{r} \neq \mathbf{r}_0$ (see eq 11).

At the surface, adsorption of segments reduces the potential energy of chain configurations. A "sticky-surface" model, employed previously,[6] will also be used here. Segments have a finite probability of adsorption, although the attractive well at the surface is infinitely deep and narrow. The binding energy of a segment relative to a solvent molecule is χ_s, in units of kT.

Segments and solvent constrained to the surface interact as two-dimensional entities with energies described by a surface equation of state. Baram and Luban[18] give a closed-form equation of state for hard discs. Once again, the entropic part of the compressibility factor is augmented by a van der Waals-type attraction. Combining the modified compressibility factor for the surface with eq 3 and 5–7 and χ_s produces the surface SCF

$$\beta U_s = -\chi_s + B_0\ln(1 - \varphi_s) + \frac{B_1\varphi_s}{1 - \varphi_s} + \sum_{i=2}^{4} B_i(\varphi_s)^{i-1} \quad (9)$$

for $\mathbf{r} = \mathbf{r}_0$ where $B_0 = 3.467\,00$, $B_1 = 5.379\,44$, $B_2 = 3.675\,99(1 - 2\alpha) - 1.912\,44$, $B_3 = 0.284\,13$, $B_4 = 0.016\,178$, and $\varphi_s \equiv \varphi(\mathbf{r}_0)$ as defined below. It is immediately apparent that the form of the SCF proposed in eq 8 and 9 introduces a complication: $U(\mathbf{r})$, $G(\mathbf{r},s)$, and $\varphi(\mathbf{r})$ are all discontinuous at the surface.

We overcome this difficulty by expressing these functions as sums of continuous and discontinuous (surface) functions, e.g.,

$$G(\mathbf{r},s) \equiv G_c(\mathbf{r},s) + \delta(\mathbf{r} - \mathbf{r}_0)G_s(s) \quad (10)$$

$$e^{-\beta U(\mathbf{r})} \equiv e^{-\beta U_c(\mathbf{r})} + \delta(\mathbf{r} - \mathbf{r}_0)e^{-\beta U_s} \quad (11)$$

$$\varphi(\mathbf{r}) \equiv \varphi_c(\mathbf{r}) + \delta(\mathbf{r} - \mathbf{r}_0)\varphi_s \quad (12)$$

where $\mathbf{r}_0 = (x,y,0)$ denotes surface positions. We combine (10) and (1) and transform the result into a surface region SCF equation[6]

$$G_c + \delta(z)G_s = e^{-\beta U}\left\{\frac{1}{6}\nabla^2 G_c + \left[\frac{1}{2} + \frac{1}{4}\mathbf{k}\cdot\nabla\right]\times \left(G_c - \frac{\partial G_c}{\partial s}\right) + \frac{1}{2}\left(G_s - \frac{\partial G_s}{\partial s}\right)\right\} \quad (13)$$

valid for $z \ll 1$. Integrating (13) over a small interval of $O(\epsilon)$ in z, keeping only $O(1)$ terms in the result and requiring that G_c and $e^{-\beta U_c}$ vary smoothly for all $z \geq 0$, we have shown that[6]

$$G_s = K_A G_c(\mathbf{r}_0,s) \quad (14)$$

where

$$K_A \equiv e^{-\beta[U_s - U_c(\mathbf{r}_0)]} \quad (15)$$

defines a partition coefficient for segments on or near the surface. Combining (14) and (15) with (4) indicates that

$$\varphi_s = K_A\varphi_c(\mathbf{r}_0) \quad (16)$$

Thus all of the surface functions are defined in terms of their continuous counterparts. Evaluating (13) in the limit $z \rightarrow 0$ and using (14) and (15) produce

$$G_c e^{\beta U_c} = \frac{1}{2}(K_A + 1)\left[G_c - \frac{\partial G_c}{\partial s}\right] + \frac{1}{4}\mathbf{k}\cdot\nabla G_c \quad (17)$$

as the surface boundary condition at $\mathbf{r} = \mathbf{r}_0$.

Eigenfunction Expansion and Ground-State Solution. One advantage of the field equation formalism is the availability of a large body of literature concerned with the development of solutions of the Schrödinger equation. Edwards[13] and de Gennes[14] were among the first to explore these opportunities. In particular, de Gennes expanded $G(\mathbf{r},s)$ in the eigenfunctions of the Schrödinger equation and considered situations in which the lowest order or ground-state eigenfunction is dominant. We have recently completed an extensive study of the ground-state solution.[6] Since that analysis plays an important role in this work,

the basic assumptions and some important results of the ground-state solution are summarized here.

Within the ground-state approximation for adsorption near a single, planar surface (variations only in the z-direction), the configuration probability becomes

$$G_c(z,s) = g(z)e^{s\lambda_0} \tag{18}$$

with e^{λ_0} as the ground-state eigenvalue. Substitution of (10)–(12) into (4) yields

$$\varphi_c(z) = \frac{\varphi_b}{e^{-\beta U_c n}} \int_0^n G_c(z,s)G_c(z,n-s)\, ds \tag{19}$$

and, with the approximation of (18), we find

$$g(z) = (\varphi_c/K)^{1/2} \tag{20}$$

with $K = \varphi_b e^{n\lambda_0+\beta U_c}$ if full equilibrium is assumed. Usually, $\varphi_c(z)$ is small enough so that $e^{\beta U_c}$ can be expanded as

$$e^{\beta U_c} \simeq 1 + v(\varphi_c - \varphi_b) + \frac{w}{2}(\varphi_c^2 - \varphi_b^2) \tag{21}$$

in which $v \equiv 8(1-2\alpha)$ and $w \equiv 2(47 + 128\alpha(\alpha-1))$ are the dimensionless excluded volume coefficients. We assume that $v(\varphi_c - \varphi_b) \ll 1$ so that $K \approx \varphi_b e^{n\lambda_0}$ is a constant in (20). By combination of (18), (20), and (21) with (2) and with $\varphi_b \ll \varphi_c$, the unity term in (21) cancels, producing

$$\frac{d^2\varphi_c}{dz^2} - \left[\frac{d\varphi_c}{dz}\right]^2 \frac{1}{2\varphi_c} - 12\left[\lambda_0 + v\varphi_c + \frac{w}{2}\varphi_c^2\right]\varphi_c = 0 \tag{22}$$

as a self-consistent equation for $\varphi_c(z)$ within the ground-state approximation.

For adsorption, $\varphi(z)$ is greatest near the surface. To keep φ_s from exceeding unity, $e^{\beta U_s}$ and $e^{\beta U_c(0)}$ are not linearized in (17). By use of (18) and (20), (17) becomes

$$\frac{1}{8\varphi_c(0)}\frac{d\varphi_c}{dz}(0) = e^{\beta U_c(0)} - \frac{1}{2}(K_A + 1)(1 - \lambda_0) \tag{23}$$

Far from the surface,

$$\varphi_c \to \varphi_b \simeq 0 \tag{24}$$

presumes that the bulk solution is dilute and the adsorbed layer has finite extent. In practical terms, (24) restricts the validity of the ground-state solution (when considered alone[6]) to situations in which no configurations begin in the bulk solution. We shall return to this point in the next section. Except for the normalization/initial condition which fixes λ_0, the problem has been fully specified.

The first integral of (22) is

$$\frac{d\varphi_c}{dz} = -\varphi_c\left[24\left(\lambda_0 + \frac{v}{2}\varphi_c + \frac{w}{6}\varphi_c^2\right)\right]^{1/2} \tag{25}$$

and a second integration gives the volume fraction profile

$$\varphi_c(z) = \frac{4\lambda_0 c_i e^{-\gamma z}}{\left(c_i - \frac{v}{2}e^{-\gamma z}\right)^2 - \frac{2}{3}\lambda_0 w e^{-2\gamma z}} \tag{26}$$

where $\gamma = (24\lambda_0)^{1/2}$ and

$$c_i = \frac{1}{\varphi_c(0)}\left\{2\lambda_0^{1/2}\left[\lambda_0 + \frac{v}{2}\varphi_c(0) + \frac{w}{6}\varphi_c^2(0)\right]^{1/2} + \frac{v}{2}\varphi_c(0) + 2\lambda_0\right\} \tag{27}$$

is an integration constant. Equations 8, 9, 15, 16, 23, and 25 are evaluated at $z = 0$ and solved for $\varphi_c(0)$; c_i is then evaluated through (27).

Matched Asymptotic Expansion. The ground-state solution (26) of the self-consistent field equation (22) is an informative but incomplete characterization of an adsorbed polymer layer. Consider the contribution to the volume fraction by segments of specific rank or contour location within the chain:

$$\varphi_c(z,s) \equiv \varphi_b G_c(z,s)G_c(z,n-s) \tag{28}$$

i.e., the integrand of (4). Substitution of the ground-state form (18) into (28) produces $\varphi_c(z,s) \simeq \varphi_b g^2(z)e^{n\lambda_0}$, which is independent of s. Thus there are no end effects, precluding the prediction of tails. Consequently, the ground-state predictions for the total adsorbed amount of polymer and the layer thickness are significantly less than those found experimentally.

A more realistic representation of an adsorbed layer recognizes the fundamental differences between the layer structure close to and far from the surface. Distinction between structural regions has appeared in the context of scaling theory,[19] so its use here is not without precedent. Near the surface where the volume fraction is high and the ground-state solution is presumably accurate, adsorption and interchain interactions distort chains from their ideal configurations. The relevant characteristic length is the statistical segment length. Far from the surface, chain configurations are similar to those in bulk solution. If the solution is not too concentrated, the chains are ideal and the characteristic length is proportional to the square root of the chain length. This length scale is much larger than the segment length for long chains.

Because the length scales are well-separated, we can regard the ground-state solution as an "inner region" solution which must be asymptotically matched to an "outer region" solution found on the length scale given by $n^{1/2}$. In formal terms, the contour length and distance from the surface are rescaled so that $t = s/n$ and $x = z/n^{1/2}$. Equation 2 becomes

$$\frac{\partial G_c}{\partial t} = \frac{1}{6}\frac{\partial^2 G_c}{\partial x^2} + n[1 - e^{\beta U(x)}]G_c \tag{29}$$

Choosing $\epsilon = 1/n$ as a small parameter, G_c is expanded in a regular perturbation series as

$$G_c = G_0 + \epsilon G_1 + \ldots \tag{30}$$

Equation 21 indicates that $n(1 - e^{\beta U_c}) \simeq -nv(\varphi_c - \varphi_b)$, which, inserted with (30) into (29), yields a hierarchy of independent partial differential equations, one for each power of ϵ. The lowest order equation

$$\frac{\partial G_0}{\partial t} = \frac{1}{6}\frac{\partial^2 G_0}{\partial x^2} \tag{31}$$

is simply the diffusion equation if we assume that $nv(\varphi_c - \varphi_b) \ll 1$ in the outer region. Chain configurations in the outer region are ideal at this level of approximation.

In bulk solution, chains may start anywhere with equal probability so that $G_0(x,0) = 1$. Also, G_0 must be constant in bulk solution, giving $G_0(\infty,t) = 1$. Finally, substituting (30) into a rescaled form of (17) shows that $G_0(0,t) = 0$.

The solution of the diffusion equation which satisfies these boundary conditions is simply an error function, as may be found through Laplace transforms, similarity solutions, or other techniques. The scaling cancels out of the similarity solution so that

$$G_0(z,s) = \text{erf}\,[z6^{1/2}/2s^{1/2}] \tag{32}$$

for the outer region. The inner region solution is given by (18) combined with (20), (26), and (27). A uniformly valid approximate solution is the sum of the two asymptotic

solutions, less any common terms that appear in the solutions in the appropriate limits of each. To obtain the composite solution, we note that as $z \to 0$, $G_0 \to 0$, and as $z \to \infty$, $G_{gs} \equiv g(z)e^{s\lambda_0} \to 0$; i.e., the common terms are zero. The approximate matched solution is simply the sum

$$G_c(z,s) = G_{gs}(z,s) + G_0(z,s) = g(z)e^{s\lambda_0} + \text{erf}\,[z6^{1/2}/2s^{1/2}] \quad (33)$$

since no common terms appear.

Equation 19 gives $\varphi_c(z)$ in terms of $G_c(z,s)$ for the case of full equilibrium; we also presume that $e^{-\beta U_c} \simeq 1$ and evaluate the integral in (19) analytically by recognizing the right-hand side as a Laplace transform convolution with the chain length, n, as the transform variable. Writing the transform of (19) as

$$\mathcal{L}\left\{\frac{\varphi_c n}{\varphi_b}\right\} = \tilde{G}_c{}^2(z,\eta) \quad (34)$$

with $\tilde{G}_c(z,\eta) = \mathcal{L}\{G_c(z,n)\}$, substituting the transform of (33) into (34), and inverting yield

$$\varphi_c(z) = \frac{\varphi_b}{n}\mathcal{L}^{-1}\{\tilde{G}_{gs}{}^2 + 2\tilde{G}_{gs}\tilde{G}_0 + \tilde{G}_0{}^2\} \quad (35)$$

with

$$\tilde{G}_{gs} = \frac{g(z)}{\eta - \lambda_0}, \qquad \tilde{G}_0 = \frac{1}{\eta}[1 - e^{-z(6\eta)^{1/2}}]$$

In (35) we can identify contributions to the volume fraction due to configurations with two, one, or zero sequences of segments originating in the inner region. Our conclusions regarding the ground-state solution suggest that the first term is dominated by segments contained in loops. The second and third terms correspond to segments contained in tails and nonadsorbed chains. With the individual contributions to the total polymer volume fraction labeled as φ_L, φ_T, and φ_N, (35) becomes

$$\varphi_c(z) = \varphi_L(z) + \varphi_T(z) + \varphi_N(z) \quad (36)$$

with

$$\varphi_L(z) = \frac{4\lambda_0 c_i e^{-\gamma z}}{\left(c_i - \frac{\upsilon}{2}e^{-\gamma z}\right)^2 - \frac{2}{3}\lambda_0 w e^{-2\gamma z}} \quad (37)$$

identical with the ground-state solution (26)

$$\frac{\varphi_T(z)}{\varphi_b} = \frac{2g(z)}{n\lambda_0}\left\{e^{n\lambda_0}\left[1 - \frac{1}{2}(E_1 + E_2)\right] - \text{erf}\left[\frac{z6^{1/2}}{2n^{1/2}}\right]\right\} \quad (38)$$

with

$$E_1 = e^{-(6\lambda_0)^{1/2}z}\,\text{erfc}\left[\frac{z6^{1/2}}{2n^{1/2}} - (n\lambda_0)^{1/2}\right]$$

$$E_2 = e^{(6\lambda_0)^{1/2}z}\,\text{erfc}\left[\frac{z6^{1/2}}{2n^{1/2}} + (n\lambda_0)^{1/2}\right]$$

for tails and

$$\frac{\varphi_N}{\varphi_b} = 1 - 2\left[1 + \frac{3z^2}{n}\right]\text{erfc}\left[\frac{z6^{1/2}}{2n^{1/2}}\right] + 2\left[\frac{6}{\pi n}\right]^{1/2} z e^{-3z^2/2n} + \left[1 + \frac{12z^2}{n}\right]\text{erfc}\left[\frac{z6^{1/2}}{n^{1/2}}\right] - 2\left[\frac{6}{\pi n}\right]^{1/2} z e^{-6z^2/n} \quad (39)$$

for segments belonging to nonadsorbed chains.

All that remains is the question of normalization which determines λ_0. The adsorbed amount φ_{ads} is defined by

$$\varphi_{ads} \equiv \int_0^\infty [\varphi_c(z) - \varphi_N(z)][1 + \delta(z)K_A]\,dz \quad (40)$$

or by

$$\varphi_{ads} \equiv \frac{\varphi_b}{n}\int_0^\infty \int_0^n [G_{gs}(z,s)G_{gs}(z,n-s) + G_{gs}(z,s) \times G_0(z,n-s) + G_0(z,s)G_{gs}(z,n-s)][1 + \delta(z)K_A]\,ds\,dz \quad (41)$$

after combination with (19) and (33). All segments, regardless of their rank within a chain, must contribute equally to the adsorbed amount.[5] In other words, segments can be counted up via (41), or they can be tallied, say, by counting chain ends and multiplying by the number of segments per chain. Mathematically, we have

$$\varphi_{ads} = \varphi_b \int_0^\infty [G(z,n) - G_0(z,n)]\,dz \quad (42)$$

The total solution (33) is normalized when a value of λ_0 is selected so that (41) and (42) yield the same adsorbed amount.

The configuration integral for adsorbed chains is defined as

$$Z_A \equiv \int_0^\infty [G(z,n) - G_0(z,n)]\,dz = \int_0^\infty G_{gs}(z,n)[1 + \delta(z)K_A]\,dz \quad (43)$$

where the contribution of nonadsorbed configurations is subtracted from the total configuration probability in the first expression; (10) and (33) are used to produce the second form. Equation 42 then gives

$$Z_A = \varphi_{ads}/\varphi_b \quad (44)$$

as a formal expression of equilibrium between the adsorbed layer and bulk solution.

Results and Discussion

Determination of Model Parameters. The validity of any polymer adsorption model is based on its ability to predict experimental observations. The task at hand, then, is to express the conditions and results of adsorption experiments in terms of model parameters and predictions.

We denote C_∞, M, m_b, l_b, and $\tilde{v}$ as the polymer characteristic ratio, molecular weight, molecular weight per chemical bond, average bond length, and specific volume, respectively. Quantities related to the polymer–solvent pair are the Flory entropy parameter, ψ_1, and the "theta" temperature, Θ. With $\langle r^2\rangle_0$ and r_{max} as the mean-squared end-to-end distance and the maximum extended length of a freely jointed chain, the relations $\langle r^2\rangle_0 = C_\infty n_b l_b{}^2 \equiv nl^2$ and $r_{max} = n_b l_b \equiv nl$ can be solved for n and l in terms of l_b and $n_b \equiv M/m_b$. Thus

$$l = C_\infty l_b \quad (45)$$

and

$$n = M/C_\infty m_b \quad (46)$$

are the statistical segment length and the number of segments per chain (i.e., dimensionless chain length). If we require that real polymer molecules and chains of segments have the same physical volume, then the volume per segment is

$$\upsilon_1 = \tilde{v}C_\infty m_b/N_A \quad (47)$$

where N_A is Avogadro's constant. Next, c_b, the polymer

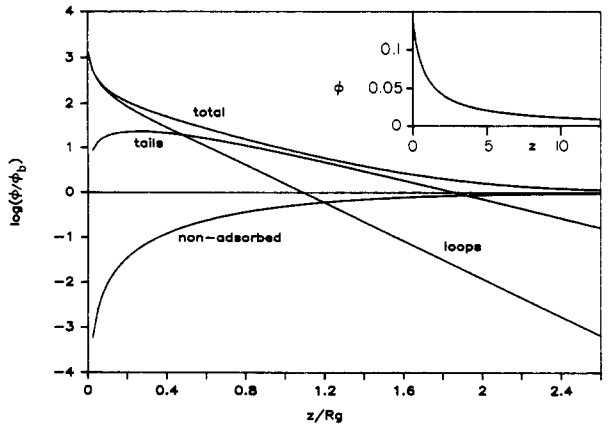

Figure 1. Polymer volume fraction profiles: φ_c is scaled on φ_b and is plotted on a logarithmic scale. Distance from the surface (in segment lengths) is scaled on the radius of gyration of an ideal chain. The top curve is the total profile for all segments, and the other curves, as indicated, are profiles for segments contained in loops, tails, and nonadsorbed chains. The total polymer volume fraction on a linear scale as function of distance from the surface is shown in the inset. Parameters include $n = 10^4$, $\chi_s = 1$, $\chi_F = 0.5$, and $\varphi_b = 10^{-4}$.

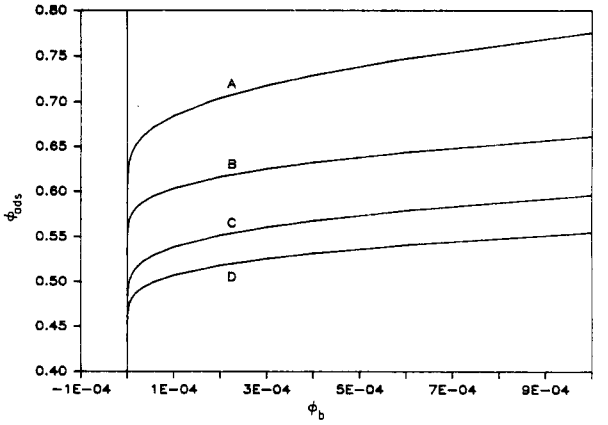

Figure 2. Adsorption isotherms for two chain lengths and two solvent qualities: (A) $n = 10^4$, $\chi_F = 0.50$; (B) $n = 10^4$, $\chi_F = 0.40$; (C) $n = 10^3$, $\chi_F = 0.50$; (D) $n = 10^3$, $\chi_F = 0.40$. Also $\chi_s = 1$.

concentration in bulk solution (mass per volume), and Γ, the polymer adsorbance (mass per area), are related to the corresponding theoretical quantities through

$$\varphi_b = c_b\tilde{v} \tag{48}$$

and

$$\varphi_{ads} = \frac{\Gamma\tilde{v}}{C_\infty l_b} \tag{49}$$

Flory's definition[15]

$$\chi_F = \frac{1}{2} - \psi_1\left(1 - \frac{\Theta}{T}\right) \tag{50}$$

gives the solvent quality parameter χ_F as a function of temperature T. The interaction parameter α that appears in (8) and (9) is related to the experimentally determined χ_F by matching the second virial coefficient so that

$$v = 1 - 2\chi_F = 8(1 - 2\alpha) \tag{51}$$

Hence $\alpha = \chi_F = {}^1/_2$ and $v = 0$ at the Θ temperature $T = \Theta$. Finally, the adsorption energy of segments relative to solvent, χ_s, has not been measured directly; we fix χ_s using one experimental measurement of adsorbed amount and then see if the model has predictive ability for other conditions of interest.

Volume Fraction Profiles of Segments. Apart from two constants, c_i and λ_0, which are found as the zeroes of two nonlinear equations, the volume fraction profiles expressed in (36)–(39) are analytical and easily evaluated. Typical profiles are shown in Figure 1; the parameters roughly correspond to 5.3×10^6 molecular weight polystyrene adsorbing from cyclohexane at the $T = \Theta$ with $\chi_s = 1.0$. φ is scaled on φ_b and plotted on a logarithmic scale to magnify the details at low volume fraction; a linear scale is used in the inset. Distance from the surface, in segment lengths, is scaled with the radius of gyration of an ideal chain, $R_g = (nl^2/6)^{1/2}$. The total volume fraction of segments is highest near the surface but decreases sharply over a narrow region that extends to a distance of about ${}^1/_3R_g$. This inner region is apparently dominated by segments contained in loop configurations.

Farther from the surface, in an outer region extending from about $0.80R_g$ to $1.8R_g$, $\varphi(z)$ decays slowly; the profile consists mainly of segments contained in tail configurations. The tail profile has a maximum near the surface reminiscent of previous solutions for terminally anchored chains.[2,31] Beyond about $2.5R_g$, nonadsorbed segments make up most of the total as the adsorbed layer merges into the bulk solution. Segments near the surface almost always belong to adsorbed chains, while segments of nonadsorbed chains are depleted there. In a sense, the surface is a "sink" for nonadsorbed chain probability and a "source" of adsorbed chain probability.

The theoretical volume fraction profiles are in qualitative but not quantitative agreement with profiles measured through neutron scattering.[37] Within the context of mean field theory, models such as the present one and that of Scheutjens and Fleer can account for the effects of adsorption energy, solvency, and excluded volume on layer structure. Effects arising from complex phenomena such as surface heterogeneity or directional polar association cannot be accomodated. Such behavior has been reported, for example, for poly(ethylene oxide) solutions and layers.[38] Theoretical predictions and measurements for the same polymer–solvent system[37] agree in their general features, and we find the same level of agreement using the present model.

Adsorbed Amount. The adsorbed amount, φ_{ads}, defined by (41), is related to the experimental polymer adsorbance through (49). Adsorbance can be measured directly by using a microbalance technique[20] and indirectly (and more easily) through a polymer mass balance based on the residual polymer concentration measured in a supernatant equilibrated with the adsorbent.

An adsorption isotherm expresses the dependence of adsorbance on the supernatant polymer concentration. Four isotherms are depicted in Figure 2 for two chain lengths and two solvent qualities. After a sharp initial increase in adsorbed amount with concentration, φ_{ads} levels off to a "pseudoplateau", in agreement with most data for monodisperse polymer. Adsorption is less in a good solvent than in a Θ solvent: when $T < \Theta$, $v > 0$ in (18), so the probability $e^{-\beta U_c(z)}$ for placing a segment at z is decreased. The unfavorable entropy loss of segment–segment contacts is manifested as an effective repulsion which increases the total free energy. The equilibrium configuration (having minimum free energy) for a layer in a good solvent is a state with fewer bound chains and fewer segment–segment contacts than in a Θ solvent, especially at the surface where φ_c is greatest.

The influence of chain length on adsorbed amount is shown more completely in Figure 3, with both φ_{ads} and n plotted logarithmically. The points are experimental data for adsorption of polystyrene on chrome[21] and silica[22,23]

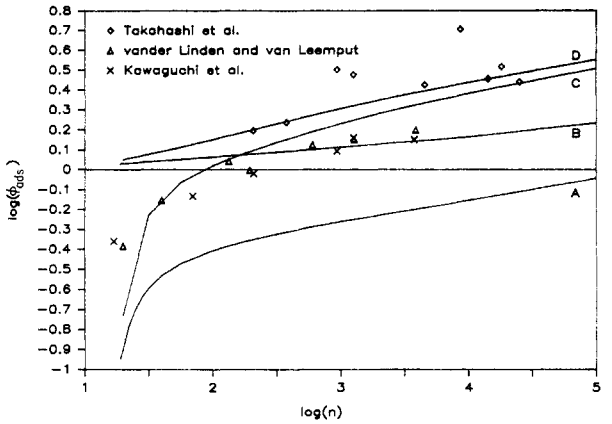

Figure 3. Adsorbed amount as a function of chain length plotted on a log–log scale. The points, as indicated, are data for adsorption of polystyrene onto chrome (Takahashi et al.[21]) and silica (vander Linden and van Leemput[22] and Kawaguchi et al.[23]) from cyclohexane at $T = \Theta \simeq 35$ °C. The curves are the predictions of the present model using two different equations of state to generate the SCF. Curves A and B (χ_s = 1 and 15) employ the SCF developed herein as given by eq 8 and 9. Curves C and D (χ_s = 1 and 15) are based on the Flory–Huggins equation of state, used in ref 6, which produces the SCF of eq 33a and 33b therein. In all cases $\chi_F = 0.50$ and $\varphi_b = 1.85 \times 10^{-4}$.

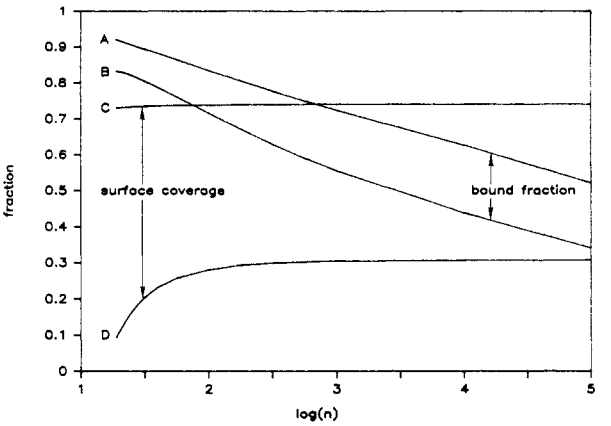

Figure 4. Bound fraction and surface coverage as functions of the logarithm of the chain length. Curves A and C are for χ_s = 10; curves B and D are for $\chi_s = 1$. Other parameters include $\chi_F = 0.50$ and $\varphi_b = 1.86 \times 10^{-4}$.

from cyclohexane at the Θ temperature; the curves are the theoretical predictions of the present model using two different equations of state. Curves A and B (χ_s = 1 and 15) are calculated by using the Carnahan–Starling/van der Waals SCF given by (8) and (9). Curves C and D (χ_s = 1 and 15) are based on the Flory–Huggins equation of state used in ref 6; the resultant SCF is given by eq 33a and 33b therein.[39] Except for χ_s, all parameters are calculated from experimental conditions through eq 45–51.

In general, adsorption increases with adsorption strength and chain length, but φ_{ads} appears to reach a limit at large n in good solvents. φ_{ads} is roughly linear in log (n) for $n > 10^4$. Selection of $\chi_s = 1.0$ produces curves (A and C) having the same features as the silica data: φ_{ads} increases steeply with n for small n and more gradually for larger n. Although the two equations of state give predictions which bracket the silica data, neither produces quantitative agreement over a significant range of n. Increasing χ_s to 15 (curves B and D) does not conclusively improve the comparison: the SCF derived herein and the Flory–Huggins SCF produce limited agreement with *different* sets of data; furthermore, some of the qualitative features of the data for $n < 1000$ are lost. Values of $\chi_s > 15$ are probably unrealistic.

The adsorption trends manifested in variations of φ_{ads} with n, χ_F, and χ_s have been found by several other theories[2-6] and are not hard to explain. Chains lose configurational entropy upon adsorption because the surface and other chains reduce the number of configurations that the chain may assume. Adsorption occurs, though, because the binding energy of segments on the surface is a favorable contribution to the total free energy. The balance between adsorption energy gain and configurational entropy loss determines the equilibrium adsorbed amount. Naturally, when the adsorption energy per segment is greater, the balance shifts toward more adsorption. Figure 4 illustrates this point. The fraction of all segments that are on the surface, $p = \varphi_s/\varphi_{ads}$ (the bound fraction), and the surface coverage, φ_s, both increase with χ_s. Configurational entropy loss per chain increases with chain length;[2] however, this loss is minimized if chains form more loops and tails which preserve configurational entropy. As n increases, additional segments are accomodated in loops and tails with little entropy penalty, so φ_{ads} increases. The results in Figure 4 support this explanation: for larger n, p falls dramatically as loops and tails become dominant. However, φ_s remains nearly constant because adsorption energy balances segment–segment repulsion at the surface. In good solvents more than in Θ solvents, the entropy penalty upon adsorption is greater due to the restrictions of other chains: hence adsorption is limited at large n.

Layer Thicknesses. Layer thicknesses are significant for practical applications and are measured through a variety of methods. One technique, ellipsometry, has been thoroughly reviewed in a number of publications.[4,24,25,35] McCrackin and Colson[35] compare the ellipsometric layer thickness, t_{el}, with the root-mean-square (rms) thickness calculated from exponential, Gaussian, and linear distributions of refractive index. de Gennes and Charmet[25] suggest that t_{el} is equivalent to the first moment of $\varphi_c(z)$. Our calculations utilize

$$t_{el} = \frac{\varphi_{ads}^2}{\int_0^\infty [\varphi_c(z) - \varphi_N(z)]^2 \, dz} \tag{52}$$

based upon McCrackin and Colson's[35] analysis of inhomogeneous films and assuming a linear relationship between $\varphi_c - \varphi_N$ and the refractive index of the polymer–solvent mixture. Theoretical predictions and measurements support this assumption[24] for low polymer concentrations and molecular weights.

Extensive ellipsometric studies of polystyrene adsorption on chrome from cyclohexzne[4,21,27] have revealed some general trends. First, t_{el} varies with polymer molecular weight as $t_{el} \approx M^a$ with $a = 0.50$ for Θ solvents and 0.40 for good solvents. Scaling theory[19,26] predicts these exponents exactly, and the SF theory[5] is in qualitative agreement. The power law scaling is evident in the data[21] shown in Figure 5 (points) for polystyrene adsorption from cyclohexane at $T = \Theta$. The present theory predicts thicknesses that are more than a factor of 3 too small and which tend to level off for large n. Calculating the thickness only of segments in tails, we find better agreement with the data; the slope is 0.53. Other experiments[27] show that while φ_{ads} is less in a good solvent than a Θ solvent, t_{el} is greater in good solvents. Our results as well as those of the SF theory[5] show the opposite trend, that t_{el} is less in a good solvent. The present model predicts t_{el} scales with $n^{0.49}$ in a good solvent.

The poor quantitative and marginal qualitative agreement between experimental and theoretical values of t_{el} cannot yet be explained unambiguously, but we can suggest

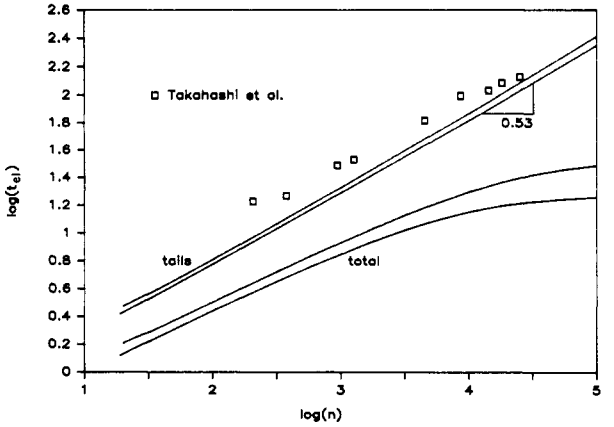

Figure 5. Ellipsometric layer thickness as a function of chain length plotted on a log–log scale. The points are the data of Takahashi et al.[21] (system as in Figure 3). The curves are the predictions of the present model: the lower pair of curves give the thickness due to all segments, and the upper pair the thickness due to segments in tails alone. Of each pair, the upper curve is for $\chi_s = 1.0$, and the lower curve is for $\chi_s = 15$. Other parameters include $\chi_F = 0.50$ and $\varphi_b = 2.78 \times 10^{-3}$.

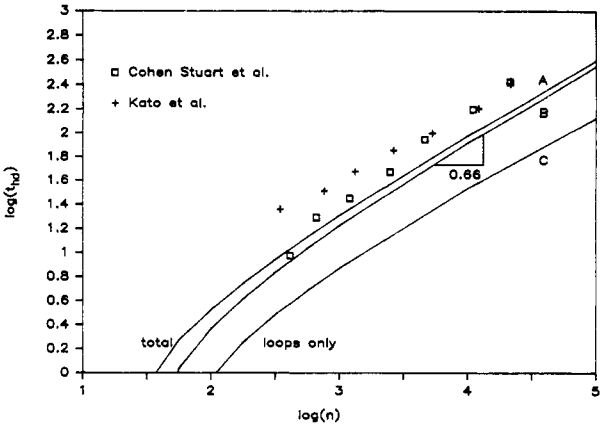

Figure 6. Hydrodynamic thickness as a function of chain length, plotted on a log–log scale. The points are the data of Cohen Stuart et al.[29] and Kato et al.[30] for adsorption of poly(ethylene oxide) onto polystyrene particles suspended in water at $T = 25$ °C (a good solvent). The curves are the predicted thicknesses of the present model: curve A ($\eta = 2$) and curve B ($\eta = 1$) give t_{hd} due to all segments (loops plus tails) and curve C ($\eta = 1$) is t_{hd} due to segments in loops alone. Parameters include $\chi_s = 1$, $\chi_F = 0.448$, and $\varphi_b = 2.38 \times 10^{-3}$.

several possible reasons. First, all of the approximations and shortcomings of the solution equation of state will also be present in the polymer adsorption theory. A poor model for the free energy density in (3) will produce an unrealistic distribution of chain configurations. Second, the conversions between experimental and model parameters may be inaccurate. For example, variation of the segment length would shift the experimental data relative to the theoretical curves, but the direction and magnitude are not obvious. Finally, the present model probably underestimates the average loop length, especially at large n. This possibility will be discussed in more detail in the next section.

Hydrodynamic methods, such as dynamic light scattering (DLS) or capillary viscometry, provide another means of characterizing the layer thickness. The hydrodynamic thickness, t_{hd}, is not simply related to a moment of φ_c. Instead, t_{hd} characterizes the effect of a polymer layer on an imposed weak flow of solvent through the layer. For example, the difference between the apparent radius of colloidal particles (found through DLS) measured before and after polymer adsorption gives t_{hd}. Theoretical models of weak solvent flow through adsorbed layers[28] assume that the chain configurations are unperturbed by the flow. The solvent velocity profile satisfies the Debye–Brinkman equation, a form of the Navier–Stokes equation that reduces to Darcy's law when the layer permeability is low (i.e., $\varphi \to 1$). The details of the calculations can be found elsewhere;[6] for now, we only mention that the segments interact hydrodynamically and that the drag on each segment is that of an equivalent Stokes sphere with diameter η in units of segment length.

Figure 6 is a log–log plot of t_{hd} as a function of n. The points are the thicknesses measured by Cohen Stuart et al.[29] and Kato et al.[30] by DLS for adsorption of poly(ethylene oxide) on polystyrene particles suspended in water at 25 °C (a very good solvent for PEO). Both groups find $t_{hd} \approx n^a$ with $a = 0.80$ (ref 29) or $a = 0.56$ (ref 30). The values of t_{hd} calculated from the present adsorption theory and our earlier solvent flow model[6] agree well with the data; t_{hd} is about half of the measured values and $a = 0.66$. Similar agreement is achieved by Cohen Stuart et al.[29] using SF theory. The frictional resistance characterized by $\eta = 1$ is quite reasonable; furthermore, the results are not very sensitive to variations in η or χ_s. For comparison, Figure 6 also includes t_{hd} due to segments in loops alone. The hydrodynamic thickness of loops is considerably less than that due to all segments. This observation agrees with previous results[29,32] which indicate that hydrodynamic methods probe regions of the volume fraction profile where tails are dominant or, conversely, that tails are important when considering the hydrodynamic behavior of adsorbed layers.

Statistics of Loops and Tails. Manipulation of the structure and properties of an adsorbed layer through variation of experimental conditions is an importance problem that has largely been addressed on an empirical basis. The previous results suggest that the layer's structure can be interpreted through consideration of the distribution of segments in trains, loops, and tails. The sensitivity of this distribution to changes in model parameters is therefore a relevant question. The answers may suggest new experimental tests or improvements in practical systems.

Two statistical measures are the average number of loops and tails per chain. A loop is defined as a sequence of segments having two ends adsorbed and at least one segment a unit distance from the surface. Mathematically, the probability that one chain part (of length s) ends on the surface is $K_A G_{gs}(0,s)$, and the probability that the other chain part (length $n - s$) ends a segment length off the surface is $G_{gs}(1,n-s)$. Using the ground-state solution given by (18), (20), and (26), integrating over all locations within the chain, and normalizing with the configuration integral, we find

$$\langle n_L \rangle = \frac{K_A g(0) g(1) n e^{n\lambda_0}}{Z_A} \tag{53}$$

as the number of loops per chain, where Z_A is defined in (43). A similar calculation gives $\langle n_T \rangle$, the number of tails per chain. Alternately, we can count the number of ends on the surface and subtract from the maximal number of tails per chain, two, yielding

$$\langle n_T \rangle = 2\left[1 - \frac{K_A g(0) e^{n\lambda_0}}{Z_A}\right] \tag{54}$$

Calculations of $\langle n_L \rangle$ and $\langle n_T \rangle$ (not shown) indicate that they are relatively insensitive to variations in χ_s, χ_F, and φ_b compared to variations with n. In general, $\langle n_L \rangle$ is large

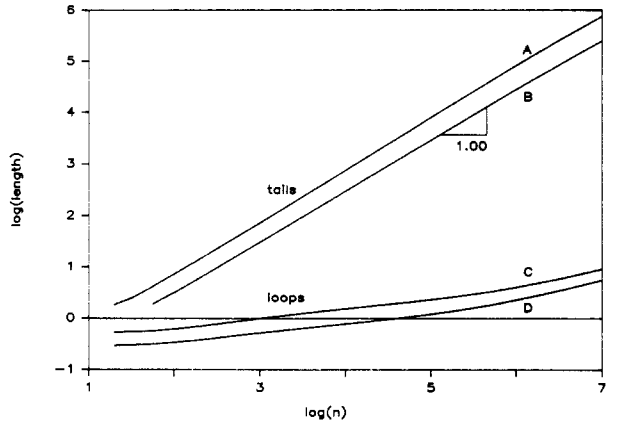

Figure 7. Average length of loops and tails as functions of chain length plotted on a log–log scale. Parameters include $\chi_s = 1$, $\chi_F = 0.50$, and $\varphi_b = 10^{-4}$, except for curve B for which $\varphi_b = 10^{-8}$ and curve D for which $\chi_s = 10$.

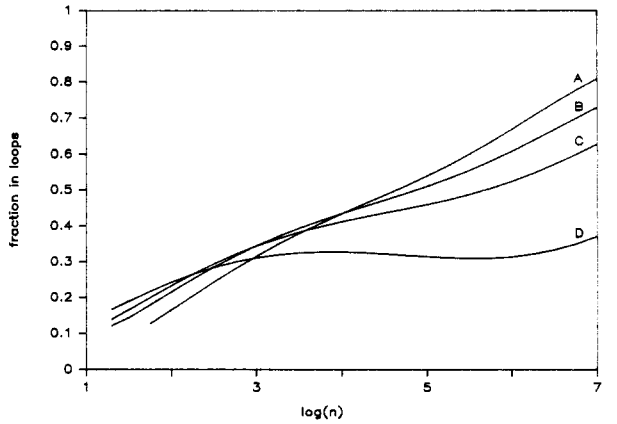

Figure 8. Fraction of segments in loops as a function of the logarithm of the chain length. Curves A, B, C, and D are for $\varphi_b = 10^{-8}$, 10^{-4}, 10^{-3}, and 10^{-2}, respectively. Other parameters include $\chi_s = 1$ and $\chi_F = 0.50$.

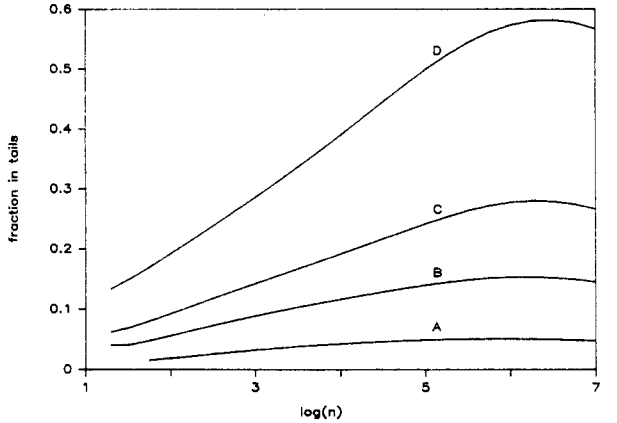

Figure 9. Fraction of segments in tails as a function of the logarithm of the chain length. Curves A, B, C, and D are for $\varphi_b = 10^{-8}$, 10^{-4}, 10^{-3}, and 10^{-2}, respectively. Other parameters include $\chi_s = 1$ and $\chi_F = 0.50$.

$(O(n/10))$] and increases monotonically with n, while $\langle n_T \rangle$ is less than one for short chains but reaches the limiting value of two for large n. These results are consistent with the view that short chains have many trains, short loops, and few tails, but longer chains have more segments in loops and tails which preserve configurational entropy.

Comparison with the results of SF theory[5,32] indicates that the present model predicts too many loops per chain. This inaccuracy is manifested in two ways. First, each term in the product $G_{gs}(0,s)G_{gs}(1,n-s)$ fails to account for the probability of tails existing at each end of the chain rather than sequences of loops and trains as required by the ground-state solution. A related source of error is the assumption that the first term in (35), rewritten as (37), represents the complete solution for segments in loops. A more accurate solution of (2) requires the retention of more terms in the eigenfunction expansion that was truncated to give (18). The present matched asymptotic solution is similar to the two eigenfunction scheme proposed by Fleer et al.[32] Higher order eigenfunctions would produce additional cross terms in (35), reducing the relative importance of the numerous short loops arising from the ground-state eigenfunction.

The average length of loops and tails may be more significant than their numbers. First, the fractions of segments in loops and tails are calculated from

$$\nu_L = \frac{1}{\varphi_{ads}} \int_0^\infty \varphi_L(z)\, dz \tag{55}$$

and

$$\nu_T = \frac{1}{\varphi_{ads}} \int_0^\infty \varphi_T(z)\, dz \tag{56}$$

Then

$$\langle L_L \rangle = \nu_L n / \langle n_L \rangle \tag{57}$$

and

$$\langle L_T \rangle = \nu_T n / \langle n_T \rangle \tag{58}$$

are the average loop and tail lengths. In Figure 7, $\langle L_L \rangle$ and $\langle L_T \rangle$ are plotted on a log–log scale as functions of chain length. The average loop is short, falling below one segment length for small n. This apparent contradiction with the definition of loops used in (53) results from the overestimation of $\langle n_L \rangle$ due to the ground-state approximation. Higher order eigenfunctions would reduce $\langle n_L \rangle$ and thus increase $\langle L_L \rangle$. $\langle L_T \rangle$ increases linearity with n in agreement with SF theory.

Of the parameters other than n, $\langle L_L \rangle$ is most sensitive to χ_s. The bound fraction, that is, the fraction of segments in trains, increases markedly with χ_s, as shown in Figure 4. The formation of more trains comes at the expense of loops, so the drop in $\langle L_L \rangle$ at higher χ_s is not surprising. As chain length increases, $\langle L_T \rangle$ grows dramatically because tails are generally more capable of preserving configurational entropy than loops. Tail length is not at all sensitive to χ_s and varies slightly with χ_F. Figure 7 shows, though, that $\langle L_T \rangle$ increases with φ_b. At all chain lengths, φ_{ads} grows with φ_b (see Figure 2); again, for entropic reasons, the extra segments go into tails. Although tails are longer after adsorption from more concentrated solutions, the number of tails increases relatively little.

Two other informative statistical measures are the fractions of segments in loops and tails, defined in (55) and (56). These quantities, presented as functions of log (n) in Figures 8 and 9, vary considerably with φ_b. Again, these trends are explained by consideration of the modes of configurational entropy preservation in adsorbing chains. When the bulk solution is dilute ($\varphi_b = 10^{-8}$), φ_{ads} is low (Figure 2) and chains are found in "loopy" configurations as suggested by the high values of ν_L and the low values of ν_T (Figures 8 and 9). As n and φ_{ads} increase (see Figure 3), p (Figure 4) decreases as chains adsorb in loop and tail configurations which preserve configurational entropy. However, when φ_b is low and φ_{ads} is relatively low (compared to values at larger φ_b), loop formation is preferred over that of tails since this distribution maximizes the number of segments in contact with the surface. Hence

ν_L grows with n while ν_T remains low.

At intermediate values of φ_b, the equilibrium distribution shifts toward the formation of more tails and fewer loops. When $\varphi_b = 10^{-2}$, the adsorbed amount is high, and tails are the dominant configuration; the total free energy is more easily minimized by reducing the entropy loss rather than by increasing the number of adsorbed segments. The tail fraction grows dramatically with n as the loop fraction reaches a local maximum and then falls. However, the distribution starts to shift back to loop formation for very long chains. Given our earlier reservations regarding the accuracy of $\langle n_L \rangle$ and $\langle L_L \rangle$, the maximum in ν_T may not exist in reality. SF theory[32] predicts that ν_T increases monotonically with n.

Conclusions

Analysis of chain configuration statistics is the most direct way of quantifying adsorbed layer structure. Although the behavior is complex, the variation of the statistical distribution of segments in trains, loops, and tails with experimental parameters can be understood in simple thermodynamic terms. The goal of free energy minimization, promoted by the formation of segment–surface contacts and by elimination of entropically unfavorable interactions, is achieved within the constraints imposed by structure and chemistry. For example, more loops and tails can be created only if fewer segments per chain adsorb on the surface. The optimal balance depends on experimental conditions and determines the structure of the adsorbed layer.

With the exception of the bound fraction, chain statistics are usually not measurable but manifest themselves in other experimentally observable quantities. Polymer volume fraction profiles, bound fraction, surface coverage, adsorbed amount, and several different layer thicknesses are accessible to experiments of varying degrees of complexity. We have compared our theoretical predictions with experimental data for the adsorbed amount, the ellipsometric thickness, and the hydrodynamic thickness. Agreement is at least qualitatively good for φ_{ads}, t_{el}, and t_{hd}. These comparisons raise a number of questions regarding the fundamental assumptions and approximations of the adsorption theory presented herein. These can be divided into three categories: assumptions upon which the general self-consistent field equation (2) is based, assumptions regarding the form of the local free energy density supplied to the model via (3), and approximations made in the course of solving the equations.

In general, contemporary adsorption theories are closely related to corresponding models of polymer solutions. Two classes of theories, the so-called "mean-field" and "scaling" approaches, have successfully interpreted experimental data for solutions. Only recently, however, have the regimes of validity for each approach been carefully delineated.[33] Scaling laws are valid in very good solvents or for very long chains in which strong intrachain segment–segment repulsions swell configurations relative to the ideal state. Above a certain crossover volume fraction $\tilde{\varphi}$, however, segments from other chains screen the intrachain interactions so that configurations are ideal on all length scales greater than the segment length. For $\varphi > \tilde{\varphi}$, fluctuations can be neglected and segment interactions may be treated by using a local mean field. The volume fraction in an adsorbed layer is usually much greater than $\tilde{\varphi}$, at least for $z < {}^1/_2 R_g$. Thus the mean-field approach used here is appropriate for much of the layer.

On the other hand, $\varphi(z)$ can be concentrated at the surface, pass through the semidilute regime in the vicinity of the surface, and merge into a dilute bulk solution. For depletion layers,[34] $\varphi(z)$ is dilute near the surface and semidilute or concentrated in bulk. No adsorption model at present encompasses all regimes of polymer concentration with high accuracy. However, when the length scale associated with the bulk solution is much greater than the characteristic length of configurations in the adsorbed layer, a matching procedure can provide a composite volume fraction profile. In the present case, a concentrated, mean-field inner solution (characteristic length $\simeq 1/\lambda_0$) is matched with an ideal, dilute outer solution (length $\simeq n^{1/2} \gg 1/\lambda_0$). Other solutions with well-separated length scales are concentrated adsorbed layers (mean-field approach) matched with concentrated bulk solutions and semidilute adsorbed layers (scaling approach[19]) matched with ideal dilute or less concentrated semidilute bulk solutions. While these cases are amenable to the matching technique, a more comprehensive model awaits further development of unified models of polymer solutions.[33]

The choice of solution equation of state is critical in determining the layer structure since the adsorption theory is only as accurate as the constituent models for segment interactions. A limited number of comparisons between results[6] based on the Flory–Huggins equation and those generated herein by using a van der Waals equation of state show that the characteristics of the adsorbed layer clearly differ in the two cases. Further progress in this area depends on the continuing development of accurate polymer solution theories as well as more extensive comparisons of solution and adsorption data with theoretical predictions.

This work demonstrates that many of the salient features of adsorbed polymer layers can be studied without resort to extensive numerical solutions. The earlier ground-state model[6] provided an incomplete description of the adsorbed layer; that solution has been extended by the present matched asymptotic solution, but further refinement is needed to achieve quantitative agreement with experimental data and other theoretical predictions. Analytical solutions become possible through a sacrifice of accuracy due to the truncation of various expansions, but most of the relevant physics of the problem are retained. The SF theory[5] provides exact solutions of (2) for a different subset of parameter space within the approximations of lattice geometry and Flory solution theory. These two approaches should be regarded as complementary solutions of the same field equation. The most important problems at present are the development of more accurate models for segment interactions which comprise the self-consistent field and resolution of questions concerning the importance of higher order terms in the eigenfunction expansion of $G(\mathbf{r},s)$.

Acknowledgment. We gratefully acknowledge the support of the Chemical Sector of the Allied Corporation. We also thank Prof. Gerard Fleer and Dr. Jan Scheutjens for their valuable comments and Kookheon Char for finding several errors in the manuscript.

References and Notes

(1) Eirich, F. *J. Colloid Interface Sci.* **1977**, *58*, 423.
(2) Hesselink, F. Th. *J. Phys. Chem.* **1969**, *73*, 3488; **1971**, *75*, 65.
(3) Chandrasekhar, S. *Rev. Mod. Phys.* **1943**, *15*, 1.
(4) Takahashi, A.; Kawaguchi, M. *Adv. Polym. Sci.* **1982**, *46*, 1.
(5) Scheutjens, J. M. H. M.; Fleer, G. J. *J. Phys. Chem.* **1979**, *83*, 1619; **1980**, *84*, 178. Scheutjens, J. M. H. M.; Fleer, G. J. *Macromolecules* **1985**, *18*, 1882.
(6) Ploehn, H. J.; Russel, W. B.; Hall, C. K. *Macromolecules* **1988**, *21*, 1075.
(7) Helfand, E. *J. Chem. Phys.* **1975**, *62*, 999.
(8) Dickman, R.; Hall, C. K. *J. Chem. Phys.* **1986**, *85*, 4108.
(9) Hong, K. M.; Noolandi, J. *Macromolecules* **1981**, *14*, 727.

(10) van Kampen, N. G. *Stochastic Processes in Physics and Chemistry*; North-Holland: New York, 1985.
(11) Freed, K. F. *Adv. Chem. Phys.* **1972**, *22*, 1.
(12) Ploehn, H. J. *Self-Consistent Field Theory of Polymer Adsorption*; Ph.D. Thesis, Princeton University, Princeton, NJ, 1988.
(13) Edwards, S. F. *Proc. Phys. Soc., London* **1965**, *85*, 613.
(14) de Gennes, P.-G. *Rep. Prog. Phys.* **1969**, *32*, 187.
(15) Flory, P. J. *Principles of Polymer Chemistry*; Cornell University: Ithaca, NY, 1953.
(16) Okamoto, H. *J. Chem. Phys.* **1975**, *64*, 2686. Croxton, C. A. *J. Phys. A: Math. Gen.* **1979**, *A12*, 2497.
(17) Carnahan, N. F.; Starling, K. E. *J. Chem. Phys.* **1969**, *51*, 635.
(18) Baram, A.; Luban, M. *J. Phys. C* **1979**, *12*, L659.
(19) de Gennes, P.-G. *Macromolecules* **1981**, *14*, 1637. de Gennes, P.-G. *Scaling Concepts in Polymer Physics*; Cornell University: Ithaca, NY, 1979.
(20) Terashima, H.; Klein, J.; Luckham, P. F. In *Adsorption from Solution*; Rochester, C. H., Smith, A. L., Eds.; Academic: London, 1983.
(21) Takahashi, A.; Kawaguchi, M.; Hirota, H.; Kato, T. *Macromolecules* **1980**, *13*, 884.
(22) vander Linden, C.; van Leemput, R. *J. Colloid Interface Sci.* **1978**, *67*, 48.
(23) Kawaguchi, M.; Hayakawa, K.; Takahashi, A. *Polym. J. (Tokyo)* **1980**, *12*, 265.
(24) Stromberg, R. R.; Passaglia, E.; Tutas, D. J. *J. Res. Natl. Bur. Stand., Sect. A* **1963**, *67*, 431. Stromberg, R. R.; Tutas, D. J.; Passaglia, E. *J. Phys. Chem.* **1965**, *69*, 3955.
(25) Charmet, J. C.; de Gennes, P.-G. *J. Opt. Soc. Am.* **1983**, *73*, 1777.
(26) de Gennes, P.-G. *Adv. Colloid Interface Sci.* **1987**, *27*, 189.
(27) Kawaguchi, M.; Takahashi, A. *J. Polym. Sci., Polym. Phys. Ed.* **1980**, *18*, 2069.
(28) Varoqui, R.; Dejardin, P. *J. Chem. Phys.* **1977**, *66*, 4395. Anderson, J. L.; Kim, J. O. *J. Chem. Phys.* **1987**, *86*, 5163.
(29) Cohen Stuart, M. A.; Waajen, F. H. F. H.; Cosgrove, T.; Vincent, B.; Crowley, T. L. *Macromolecules* **1984**, *17*, 1825. Cosgrove, T.; Vincent, B.; Crowley, T. L.; Cohen Stuart, M. A. *ACS Symp. Ser.* **1984**, *No. 240*, 147.
(30) Kato, T.; Nakamura, K.; Kawaguchi, M.; Takahashi, A. *Polym. J. (Tokyo)* **1981**, *13*, 1037.
(31) Dolan, A. K.; Edwards, S. F. *Proc. R. Soc. London, A* **1975**, *A343*, 427. de Gennes, P.-G. *Macromolecules* **1980**, *13*, 1069. Casassa, E. F. *Macromolecules* **1984**, *17*, 601. Cosgrove, T.; Heath, T.; van Lent, B.; Leermakers, F.; Scheutjens, J. *Macromolecules* **1987**, *20*, 1692.
(32) Scheutjens, J. M. H. M.; Fleer, G. J.; Cohen Stuart, M. A. *Colloids Surf.* **1986**, *21*, 285.
(33) Schaefer, D. W. *Polymer* **1984**, *25*, 387.
(34) Joanny, J. F.; Leibler, L.; de Gennes, P.-G. *J. Polym. Sci., Polym. Phys. Ed.* **1979**, *17*, 1073.
(35) McCrackin, F. L.; Colson, J. P. *NBS Spec. Publ. (U.S.)* **1964**, *256*, 61.
(36) Takahashi, A.; Kawaguchi, M.; Kato, T. *Polym. Sci. Technol. (Plenum)* **1980**, *12B*, 729.
(37) Cosgrove, T.; Heath, T. G.; Ryan, K.; van Lent, B. *Polym. Commun.* **1987**, *28*, 64.
(38) Israelachvili, J. N.; Tandon, R. K.; White, L. R. *J. Colloid Interface Sci.* **1980**, *78*, 430.
(39) In ref 6, all volume fractions in eq 33 and 40 should be multiplied by the factor ξ (defined in eq 56 of ref 6) in order to produce eq 41. The factor ξ simply rescales φ and has been eliminated in this work.

Properties of Polymer Layers Adsorbed on Surfaces under Nonequilibrium Conditions

Giuseppe Rossi* and Philip A. Pincus

Materials Department, College of Engineering, University of California, Santa Barbara, California 93106. *Received February 16, 1988; Revised Manuscript Received June 8, 1988*

ABSTRACT: The properties of polymer coated surfaces which are incompletely saturated are studied using both mean field theory and the scaling theory of polymer adsorption from a semidilute solution (in good solvents), introduced by de Gennes. We obtain theoretical predictions for the force (per unit area) between two such surfaces as a function of interplate separation. We also give the concentration profiles between the surfaces. Both in mean field and in scaling theory the results that we obtain for incompletely saturated surfaces are qualitatively different from those found in the saturated case. In particular: (i) to lowest order in mean field, interactions between incompletely saturated surfaces do not vanish (as happens in the saturated case) but rather are attractive at any interplate separation; (ii) the scaling theory predicts that, in contrast to interactions between saturated surfaces which are always repulsive in good solvents, any surface excess lower than the one corresponding to thermodynamic equilibrium will lead to attractive long distance interactions; we obtain a new set of exponents characterizing this behavior; (iii) the form of the concentration profiles as the interplate separation decreases suggests that, for incompletely saturated surfaces, bridging configurations are more favorable than nonbridging ones: this is not the case for saturated plates. An attempt has been made in this paper to spell out in some detail the experimental conditions under which our results should apply. Experimentally, attractive interplate interactions have been found: these findings agree qualitatively with our results.

1. Introduction

The interactions between polymer solutions and solid surfaces have been the subject of extensive study in recent years.[1-16] They are important in many areas of materials technology: in particular adsorbed layers of polymer are commonly used to control the stability of colloidal dispersions. Interest in this area is heightened by the fact that experimental methods[8-16] are becoming sufficiently refined to probe in detail and in a quantitative way the properties of the solid–solution interface.

Much effort has gone toward formulating theoretical treatments capable of predicting the outcome of experimental investigations. For semidilute solutions a considerable step forward in this direction occurred when de Gennes[2] extended to this problem the Cahn[17] model for interfacial tension and wetting in simple fluids. The de Gennes approach gives, in terms of a limited number of parameters, the concentration profile in proximity of the interface and the force between two polymer adsorbed surfaces. The prediction for the force plays a special role:

* Address correspondence to this author at Servizio Ricerca Centralizzata RTS, ELSAG S.p.A., 16154 Genova Sestri, Italy.

0024-9297/89/2222-0276$01.50/0